

Molecular emission from the diffuse gas around ζ Ophiuchi

H.S. Liszt

National Radio Astronomy Observatory, 520 Edgemont Road, Charlottesville, VA 22903-2475, USA

Received 7 October 1996 / Accepted 15 November 1996

Abstract. We have mapped $\lambda 18\text{cm}$ OH and $\lambda 9\text{cm}$ CH emission from the diffuse gas around ζ Oph, and find no trace of emission from the $+4.5\text{ km s}^{-1}$ gas whose OH line was previously believed to represent pre-shock gas. The pattern of OH emission is strikingly dissimilar to those of CO, HCO^+ and CH in that the strong $+1\text{ km s}^{-1}$ component seen to the South is largely absent in OH. CH more closely resembles CO, peaking on either side of the star, and comparison of CO and CH shows that the CO line ‘turns on’ over a very narrow range of CH line strength. Alternatively, OH emission actually weakens as CO brightens in the $+0.4\text{ km s}^{-1}$ line, but this may be only an excitation effect, and not the result of a declining OH abundance.

We mapped $\lambda 3\text{mm}$ HCO^+ emission over the inner portion of the gas distribution occulting ζ Oph, finding that its behaviour roughly parallels that of CO. We searched for emission from HCN, CS ($J=2-1$), CN, and C_2H at the CO and HCO^+ emission peak $30'$ South of the star. Of these, only HCN was found and it is quite weak compared to HCO^+ ($T_r^* \approx 0.03\text{ K}$ vs. 0.09 K). Emission from the other mm-wave species is absent in spectra with rms noise $\Delta T_r^* \approx 0.01\text{ K}$; CS $J=2-1$ emission was sought also unsuccessfully toward the star. The column densities inferred from these intensities are uncertain owing to unknown physical conditions along the line of sight, chiefly the kinetic temperature, but they are not necessarily much larger than would be found toward the star. Relative abundances of the high-dipole moment species are better determined; $N(\text{HCN})/N(\text{HCO}^+) \approx 1$, $N(\text{CS})/N(\text{HCO}^+) < 1$.

Key words: ISM: molecules; abundances – radio lines: ISM

1. Introduction

The diffuse or optical absorption line clouds toward the nearby (140 pc) O9 star ζ Oph offer a unique opportunity: in the apparent absence of dense gas beyond the star, the denser occulting material is clearly visible and easily isolated in radiofrequency molecular emission. The optically-determined column density and rotational excitation temperature of CO (Wannier, Jenkins

and Penzias 1982, Lyu, Smith, and Bruhweiler 1994, Lambert et al. 1994) predict a line brightness of 1–2 K at $\lambda 2.6\text{mm}$, as observed (Liszt 1992, 1993; Kopp et al. 1996). For OH (Crutcher 1979, Roueff 1996) or CH (Lien 1984; but see below) the optically-determined column densities and radio line brightness together imply typical excitation temperatures.

Radiofrequency molecular emission and optical absorption line measurements provide complementary information. Column densities, which are difficult to derive from the former, are often cleanly-determined from the latter. Line profiles, on the other hand, have until recently been obtained at much higher resolution using radiofrequency heterodyne techniques. In one interesting case, recognition of the existence of a very narrow neutral-bearing component seen in K I (Hobbs 1973) and CO (Liszt 1979), having $b = \sqrt{2}\sigma \approx 0.4\text{ km s}^{-1}$, probably caused a substantial downward revision of the very large carbon depletion factors which were at first derived toward ζ Oph (Morton 1975). But the molecular emission lines around ζ Oph are considerably broader than those arising from truly dark clouds.

At optical wavelengths, line profiles of many atomic and molecular species can now be obtained at sub- km s^{-1} resolution (Lambert, Sheffer, and Crane 1990, Crawford et al. 1994, Barlow et al. 1995, Crawford 1996). Even so, the emission observations offer three opportunities to complement the optical work. First, the gas may be traced over its spatial extent, so that we can see how the absorption line material, in otherwise anonymous diffuse clouds¹, relates to the overall spatial distribution. Second, the column density sensitivity of the mm-wave emission observations may under some circumstances substantially exceed that of the optical data, owing to the increased sensitivity of new receivers and the possibility of molecular rotational excitation by ambient electrons in diffuse gas. Last, it is possible to search in emission for species like HCO^+ (Liszt and Lucas 1994) which have either unknown or inaccessible optical spectra (Koch, van Hemert, and van Dishoeck 1995).

The appearance of the CO emission seen around ζ Oph has a very particular but not well understood behaviour whereby one or the other of the two dense kinematic components toward the star brightens within $20'-30'$ (projected distance $\approx 1\text{ pc}$) by

¹ It has already been suggested that diffuse clouds are the outer edges of centrally-condensed, darker clouds, see Federman and Willson (1982)

very large factors (Liszt 1992, 1993; Kopp et al. 1996). The star sits in a clear minimum in the integrated emission. However, given the very small amount of the total carbon column density which is in CO toward the star, $N(\text{C}^+) \approx 2 \times 10^{17} \text{ cm}^{-2}$ (Morton 1975; Cardelli et al. 1993), $N(\text{CO}) = 2.2 \pm 0.4 \times 10^{15} \text{ cm}^{-2}$ (Wannier et al. 1982; Lyu et al. 1994; Lambert et al. 1994), the increase in CO brightness above 6 K probably does not signify a similarly large increase in the extinction or total column density. Indeed, the highest CO column density which can be derived at the position of maximum CO brightness is still nearly an order of magnitude less than $N(\text{C}^+)$ toward the star (Liszt 1993; Kopp et al. 1996) and the more likely value for $N(\text{CO})$ is not more than twice what is seen toward the star. The much stronger CO emission exemplifies what can happen in the regime where CO first becomes self-shielding (*ibid*) with only a slight C^+ -CO conversion. Of course it is remarkable that 6 K CO emission might arise from a column density which represents such a small fraction of the carbon, and at $A_V = 1$ mag.

In this work, we have extended the large-scale mapping to species beside ^{12}CO , namely CH, OH, and (to a lesser extent) HCO^+ and ^{13}CO . We have also attempted to extend the recent detection of $\lambda 3\text{mm}$ HCO^+ emission around ζ Oph to other species, CN, CS, HCN, and C_2H . Of these, CN of course has a known column density in absorption $N(\text{CN}) = 2.9 \pm 0.3 \times 10^{12} \text{ cm}^{-2}$ (van Dishoeck and Black 1989) and has been sought but not seen at very low levels in mm-wave emission toward ζ Oph (Crane et al. 1989), consistent with its use as an independent indicator of the temperature of the cosmic microwave background radiation. We saw HCN at the HCO^+ emission peak, and deduce a column density comparable to or perhaps slightly greater than that of HCO^+ . A limit on the column density of CS was set from *Copernicus* data ($N(\text{CS}) < 10^{13} \text{ cm}^{-2}$; Snow 1976) and can probably be improved now; we cannot confirm the detection of CS ($J=2-1$) emission reported toward ζ Oph by Drdla, Knapp, and van Dishoeck (1989).

In Sect. 2 we discuss the new data taken for this work. In Sect. 3 we discuss maps of OH, CH, and CO and demonstrate an interesting series of relationships among the emission brightnesses of these three molecules. In Sect. 4 we derive column densities and column density limits for mm-wave emission species in the material around ζ Oph. In Sect. 5 we discuss the isotopic abundances measured in CO emission and absorption. This work is summarized briefly in Sect. 6.

2. Observations

2.1. $\lambda 18\text{cm}$ OH emission measurements

We observed the 1667.359 MHz transition of OH with the NRAO 43m antenna in Green Bank during 1995 May and September. The measured beam width of the telescope during the observations was $18.5'$ and the nominal beam efficiency was $\eta = 58\%$. Results from the 43m are reported in terms of the antenna temperature $T_A = \eta T_B$. We observed in dual circular polarization mode with 0.625 MHz correlator bandwidths in each of two 512-channel backends so that the velocity

resolution and channel separation were 0.219 km s^{-1} ; the system temperature was typically 24 K. The spectra were taken by frequency-switching and represent 9 hours on-source integration toward the star and 4.5 hours at outlying positions taken at 10-20' intervals North-South and East-West of the center position. The absolute flux scale was set by continuum observations of 3C 286.

The OH profiles are shown in Figs. 1-3 and the variation of the OH line profile integral across the face of the gas distribution is given in Table 1.

2.2. $\lambda 9\text{cm}$ CH emission measurements

We observed the 3335.481 MHz line of CH with the NRAO 43m antenna in Green Bank during 1995 September. The beamwidth of the telescope was $9.2'$. The bandwidth employed was twice as wide as for OH, which, in combination with the two times higher CH frequency, leads to a nearly identical resolution in velocity (0.219 km s^{-1}). System temperatures were 36-44K. The observing was done in quite the same way as for OH, discussed in the preceding paragraph. Integration times were 2-4 hours per position.

The CH profiles are shown in Figs. 1 and 3, and the data are summarized in Table 1.

2.3. $\lambda 3\text{mm}$ observations of HCO^+ , HCN, C_2H , CS, and CN

These data were taken at the NRAO 12m telescope in October 1994 and January 1995 using the dual-polarization receiver feeding twin banks of 100 kHz filters and the hybrid spectrometer at 97.6 kHz resolution sampled at 48.8 kHz intervals. The lines observed here are generally deserving of higher resolution but this was not feasible given the amount of observing time available. Typical integration times were 3-7 hours per point; the system temperature was 250-300 K below 100 GHz and 450 K at 113.5 GHz (for CN), all of which are worse than average for this telescope.

All these data were taken by frequency-switching and were subject to the presence of long-period sinusoidal standing waves: these have been removed from the spectra shown here. Part of the weaker hyperfine structure of HCN was lost because of our choice of a frequency-switching interval; only the strongest component could be recovered in the folded spectrum. The channel separation is 0.254 km s^{-1} for ^{12}CO , 0.258 km s^{-1} for CN, 0.266 km s^{-1} for ^{13}CO , 0.299 km s^{-1} for CS $J=2-1$, 0.328 km s^{-1} for HCO^+ , 0.330 km s^{-1} for HCN and 0.335 km s^{-1} for C_2H .

We took two additional HCO^+ emission profiles to establish the degree to which they follow the characteristic CO emission patterns. The HCO^+ data are shown in Fig. 5 and are summarized in Table 2 which gives the integrated intensities of HCO^+ and the two lower lines of ^{12}CO . The multi-species observations taken at the HCO^+ emission peak are summarized in Table 3, where we give the single-channel rms at 100 kHz resolution, the integrated intensity taken over the range defined by the relatively strong HCO^+ emission, and the fraction of the intensity of the

transition which is expected to be contained in the strongest hyperfine component. The data are shown in Fig. 6 where they are compared with observations in the core of L134 ($15^{\text{h}}51^{\text{m}}00^{\text{s}}$, $-4^{\circ}26'57''$ B1950).

2.4. New ^{12}CO , ^{13}CO , and C^{18}O $J=1-0$ profiles

Using the NRAO 12m telescope in 1995 May and July and 1996 April, new CO $J=1-0$ emission profiles were taken at $10'$ intervals in declination about the star, supplanting the earlier profiles reported in Liszt (1992). The new data were taken in a frequency-switching mode with the hybrid spectrometer. The spectra shown here have 48.8 kHz resolution and channel spacing for the stronger two isotopes (0.127 km s^{-1} for ^{12}CO , 0.132 km s^{-1} for ^{13}CO) and 97.6 kHz (0.267 km s^{-1}) for C^{18}O .

We integrated for periods of 1-3 hours on the ^{12}CO line, leading to noise levels $\Delta T_{\text{r}}^* \approx 0.035-0.07\text{K}$. For ^{13}CO , we took (four) profiles at declinations displaced $-20'$, $-10'$, $20'$, and $30'$ from the star, integrating for periods of 3-5 hours with resulting noise levels of 0.02-0.03K. For C^{18}O , we integrated for a total of 11 hours at the position $-20'$ South of the star, resulting in a single-channel rms of 0.005 K.

The newer CO results are reported in Tables 1 and 2. The ^{13}CO lines have integrated intensities identical to those reported earlier, well within the expected noise levels. Some of the ^{12}CO lines are brighter in the newer data by 20%-30% which is outside the expected noise but not inconsistent with the 10% overall calibration errors of mm-wave emission work and with the substantial upgrading of the telescope that has taken place since the first of the earlier data was taken in 1987. The newer data have slightly larger $^{12}\text{CO}/^{13}\text{CO}$ intensity ratios but the main result, that this ratio is relatively large for such strong ^{12}CO lines as are seen around ζ Oph, (up to 6.6 K), is of course preserved.

The ^{12}CO emission around ζ Oph is quite extended (de Geus, Bronfman, and Thaddeus 1990; de Geus and Burton 1991) and heavily structured (Liszt 1992, 1993; Kopp et al. 1996). We will usually assume that the forward response is filled. The nominal beam efficiency of the 12m telescope in the $\lambda 3\text{mm}$ band is 0.7.

2.5. Conventions

The central position was taken as $16^{\text{h}}34^{\text{m}}24^{\text{s}}$, $-10^{\circ}27'58''$ (B1950). At the usually-adopted distance to the star, 140 pc, $1'$ corresponds to 0.041 pc, or 1 pc to $24.6'$. All velocities reported here are with respect to the Local Standard of Rest (for conversion to heliocentric, subtract 13.7 km s^{-1} from the LSR values). The antenna temperature scale at the 12m is T_{r}^* , supposedly corrected for all losses and for all beam coupling factors other than that which describes the filling of the forward response by the actual emission. For the 43m, all results are reported in terms of the antenna temperature T_{A} . At cm-wavelengths, atmospheric attenuation is negligible and all line strengths were calibrated by observing the continuum emission from 3C 286.

3. Large-scale emission patterns of CH, OH, and CO

The large-scale molecular emission pattern immediately around ζ Oph has heretofore been studied only in ^{12}CO (Liszt 1992, 1993; Kopp et al. 1996). There is a peculiar behaviour by which one or other of the kinematic components seen toward the star at -0.7 km s^{-1} and $+1 \text{ km s}^{-1}$ brightens considerably within $20'$ (projected distance 1 pc) in the North-South direction while less structure is evident East-West. Elements of this pattern are repeated in OH and CH, although with some striking variations. The pattern is also evident in HCO^+ emission, as discussed in Sect. 4.

3.1. CH emission and excitation

The standard formula relating the CH column density to observable parameters at 3335MHz is (Mattila 1986)

$$N(\text{CH}) = C_{\text{CH}} \frac{T_{\text{ex}}}{T_{\text{ex}} - T_{\text{cmb}}} \int \frac{T_{\text{A}}}{\eta} dv \quad (1)$$

where $C_{\text{CH}} = 2.9 \times 10^{14} \text{ cm}^{-2} (\text{K km s}^{-1})^{-1}$. However, the most accurate value of $N(\text{CH})$ is that determined optically toward the star (Lien 1984), $\log N(\text{CH}) = 13.36$. It is currently believed possible to relate the CH integrated intensity directly to extinction (Mattila 1986; Magnani and Onello 1995). The mean relation of Mattila (1986) determined toward two dark clouds, $N(\text{CH}) = 4.5 \times 10^{13} \text{ cm}^{-2} (A_{\text{V}} - 0.3)$ (for $A_{\text{B}} = (4/3.1)A_{\text{V}}$), fits the current data quite well; the threshold of 0.3 mag for CH formation corresponds to the long-known sudden increase in $N(\text{H}_2)$ as it becomes self-shielding. In this case, the small variation in $\int T_{\text{A}}(\text{CH})dv$ across the face of the ζ Oph gas distribution (Table 1) is evidence that the wide swings in CO and HCO^+ intensity are excitation and chemical effects within a nearly fixed total gas column. CH peaks in the higher-velocity line to the South of the star, as does CO, but emits most strongly to the North, like OH (Figs. 1-3).

Lien (1984) attempted to derive the CH excitation temperature directly by comparing column densities in absorption; he also compared the optical and radio-determined column densities to derive the excitation temperature. Unfortunately his results were somewhat equivocal, in part owing to his use of a smaller integrated line intensity than found here and perhaps because he attempted to derive the beam efficiency in a rather circuitous manner. For $\int T_{\text{A}} dv = 0.0922 \text{ K km s}^{-1}$ toward ζ Oph (Table 1) and using equation (1) it is possible to relate the unknown excitation temperature and beam efficiency. The $\eta - T_{\text{ex}}$ locus for CH runs between ($\eta = 0.6$, $T_{\text{ex}}(\text{CH}) = -2.92 \text{ K}$) and ($\eta = 1$, $T_{\text{ex}}(\text{CH}) = -16.5 \text{ K}$). Thus the Λ -doublet in CH appears to be inverted, and it, like OH and CO, cannot be employed as a thermometer. However, this result is unexpected because the usual understanding of negative excitation temperatures in CH invokes neutral-particle collisions (Bertojo, Cheung, and Townes 1976), while the excitation of CH toward ζ Oph should be dominated by electrons, as discussed for OH in the next section.

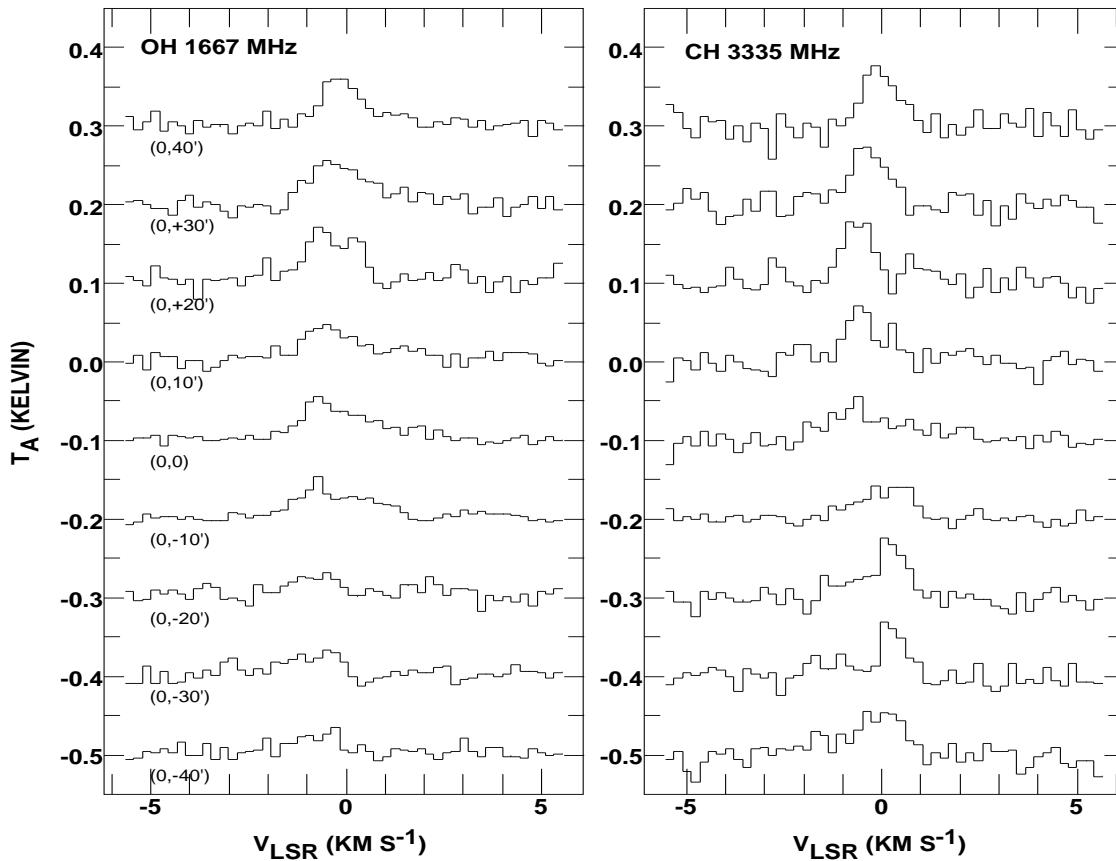


Fig. 1. Right: Line profiles of 1667 MHz OH (left) and 3335 MHz CH emission around ζ Oph. The spectral resolution of the data is 0.22 km s^{-1} . CH resembles CO, rather than OH, in the higher-velocity gas to the South.

3.2. OH emission and excitation

The $18'$ resolution OH spectra are shown in Figs. 1-3. Surprisingly, we were unable to detect a $+4.5 \text{ km s}^{-1}$ component toward the star. Given the appearance of this feature in the one earlier work where it was seen (Crutcher 1979), we are inclined to regard it as spurious. We know of nothing in our observing which might have precluded its detection (it was not corrupted by our frequency-switching interval). It seems clear from Crutcher's spectra that strongly OH-emitting gas at $+4.5 \text{ km s}^{-1}$ exists along lines of sight which are well removed from the star, but, apparently, not near it; there is a modest atomic absorption component toward ζ Oph (Hobbs 1969) at this velocity.

As noted by Black (1995, private communication) the supposed OH column density in this material was large enough ($N(\text{OH}) \approx 10^{13} \text{ cm}^{-2}$) that the absence of a stronger $+4.5 \text{ km s}^{-1}$ component in optical absorption spectra was something of a mystery. The $+4.5 \text{ km s}^{-1}$ emission was ascribed by Crutcher (1979) to gas which had been shocked by a stellar outflow, giving impetus to the study of CH^+ formation mechanisms driven by interstellar shocks. Such models are no longer believed capable of providing the values $N(\text{CH}^+) \gtrsim 10^{13} \text{ cm}^{-2}$ which are commonly observed (Allen 1994; Barlow et al. 1995) and the absence of the putative pre-shock gas probably does not

represent a real impediment to our understanding. The most recent models of CH^+ formation invoke energy dissipation which occurs in turbulent (diffuse) clouds having moderate density and $N(\text{C}^+) \gg N(\text{CO})$ (Falgarone, Pineau des Forêts, & Roueff 1995; Hogerheijde et al. 1995; Federman et al. 1996).

Another feature which is not well-represented in the OH emission spectra is the strong, higher-velocity component of the CO and HCO^+ distribution, especially near its peak $20'$ - $30'$ to the South of ζ Oph. Although the lower-velocity line shows about the same behaviour in CO and OH, its counterpart is manifested in OH only near ζ Oph. OH in the higher-velocity feature seems limb-brightened, suggesting that it exists or is excited only on the periphery of the host gas. A more extended map of the OH might detect OH emission at the southern edge of the gas as well.

The column density of OH is related to other quantities as in equation 1, substituting $C_{\text{OH}} = 2.24 \times 10^{14} \text{ cm}^{-2} (\text{K km s}^{-1})^{-1}$ from Dickey, Crovisier, and Kazès (1981). For observations toward the star, reconciliation of the observed $\lambda 18 \text{ cm}$ OH emission intensity ($0.103 \text{ K km s}^{-1}/\eta$) and the optical absorption-line column density ($4.8 \times 10^{13} \text{ cm}^{-2}$) requires a combination of beam efficiency, excitation temperature, and optical depth which lies on a locus whose limits are ($\eta = 0.58$, $T_{\text{ex}}(\text{OH}) = 16.1 \text{ K}$, $\tau(\text{OH}) = 0.007$) and ($\eta = 1$, $T_{\text{ex}}(\text{OH}) = 5.3 \text{ K}$, $\tau(\text{OH}) = 0.02$); un-

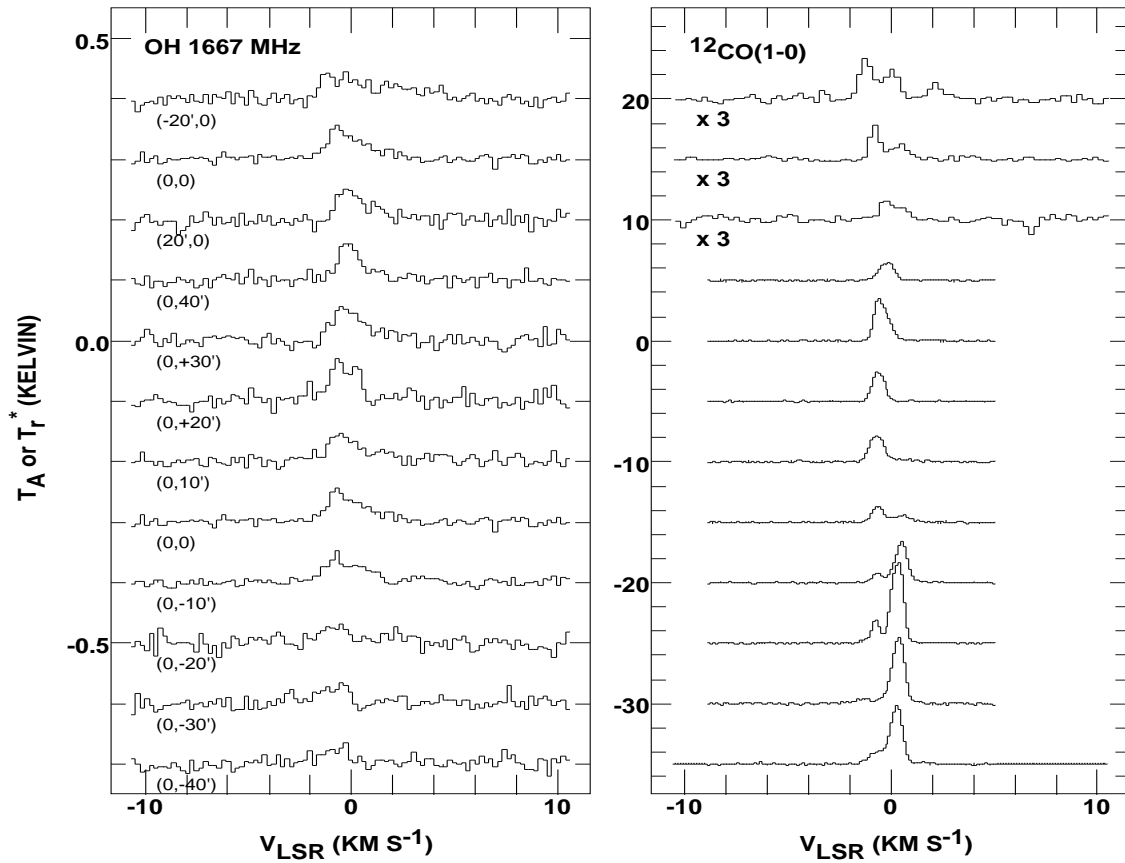


Fig. 2. Right: Line profiles of 1667 MHz OH (left) and 115.3 GHz CO emission around ζ Oph. The spectral resolution of the OH data is 0.22 km s^{-1} . For ¹²CO the spectral resolution is 0.13 km s^{-1} along the North-South strip, using newer data, and 0.26 km s^{-1} otherwise.

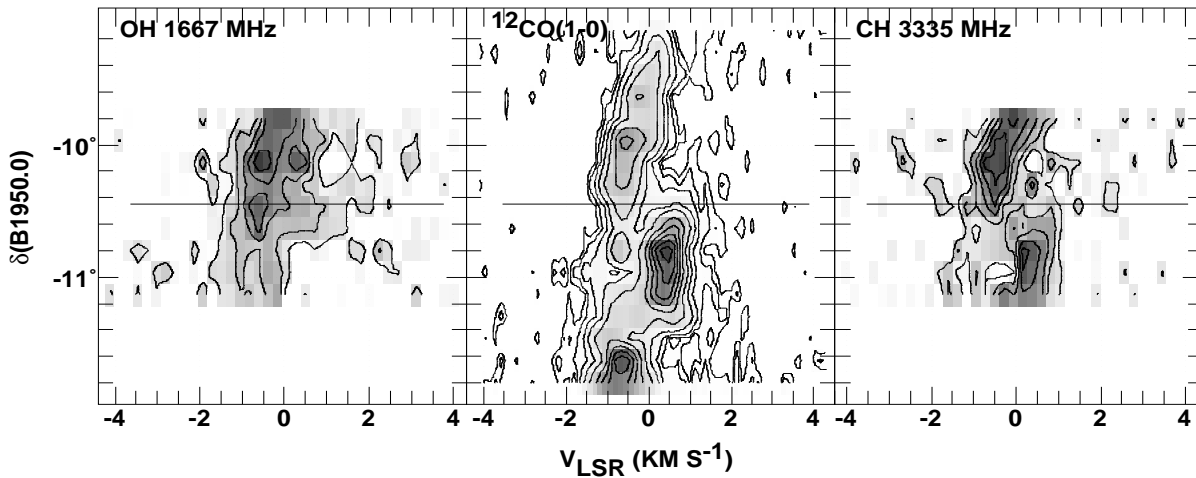


Fig. 3. Declination-velocity diagrams of OH, ¹²CO and CH emission around ζ Oph using the data in Figs. 1 and 2. The OH contours are in 0.012 K increments starting at 0.012 K; those of ¹²CO are at levels 0.0625, 0.125, 0.25, 0.5, 1, 2, 3, 4, 5, and 6 K. The CH contours are at increments of 0.014 K starting at 0.014 K. The spectral resolution is 0.22 km s^{-1} for OH and CH and 0.13 km s^{-1} for ¹²CO. The position of ζ Oph is marked by a horizontal line.

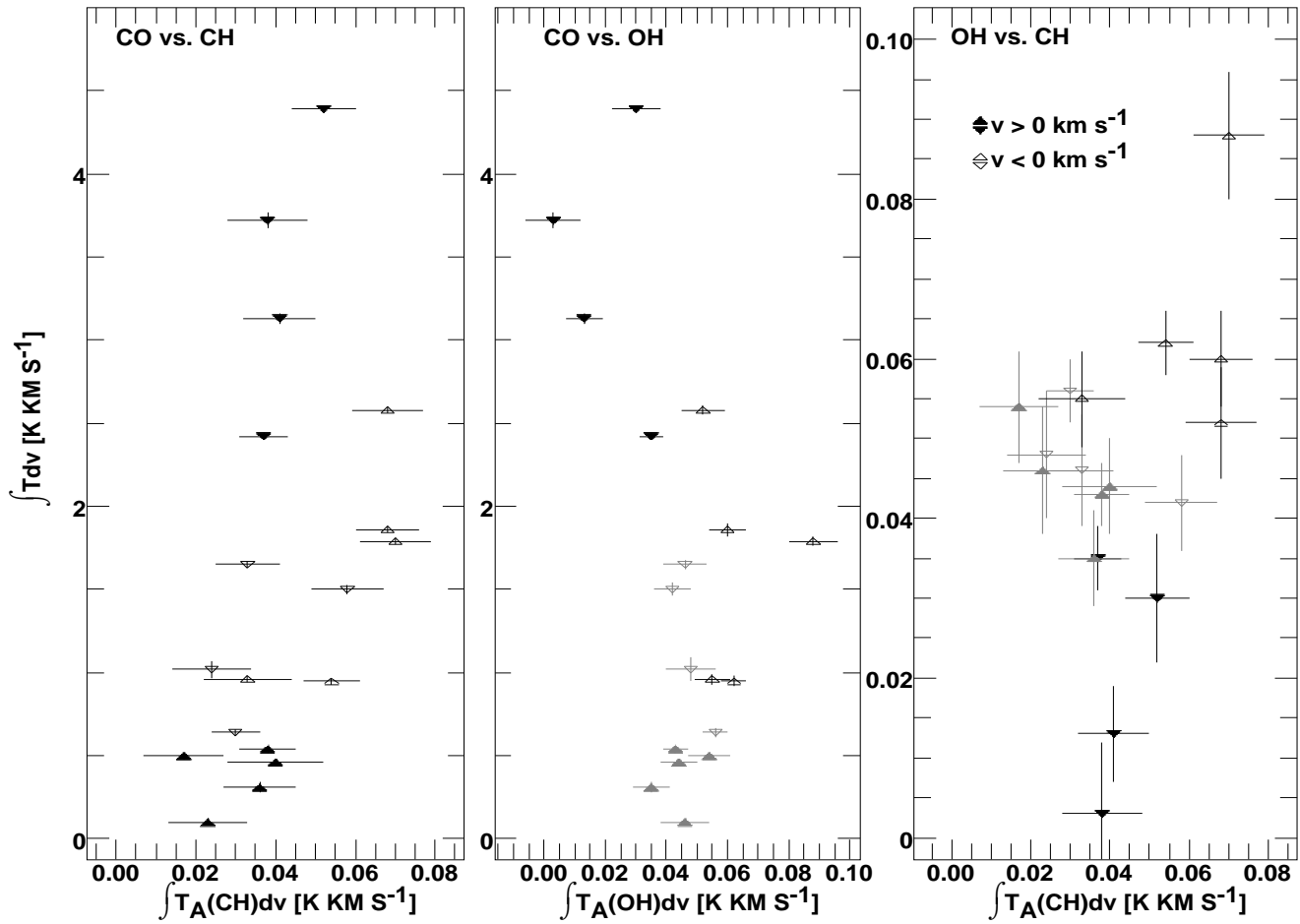


Fig. 4. Comparison of line profile integrals for CO, CH, and OH. Filled symbols are used for the integral taken at $v > 0 \text{ km s}^{-1}$, open symbols are used for $v < 0 \text{ km s}^{-1}$. Upward-pointing symbols denote positions toward or North of ζ Oph, downward-pointing symbols represent positions to the South. Symbols corresponding to the weaker of the CO emission branches are drawn less heavily in the two rightmost panels to distinguish their behaviour.

like CO there is no strong central minimum in the OH emission distribution, so that $\eta > 1$ seems unlikely. The lower of these excitation temperatures is comparable to T_{ex} for CO. Roueff (1996) derived $T_{\text{ex}}(\text{OH}) = 0.8 \pm 3.6 \text{ K}$ by comparing OH lines in absorption as Lien (1984) did for CH. She attributed this result to pumping by IR radiation, since it is so much lower than any possible kinetic temperature (see just below).

The electron density (Savage, Cardelli, and Sofia 1992) derived from the ionization equilibrium of Mg and Fe is $n(e) = 0.046 \text{ cm}^{-3}$ and the ratio of electron and radiative de-excitation rates across the ground-state Λ -doublet is $\gamma_{e-\text{OH}}/A_{\text{OH}} = 530 * (3.35 + \ln T_{\text{K}}) / \sqrt{T_{\text{K}}} \gg 1$ (Bouloy and Omont 1978). If these electrons are mainly contributed by carbon, $n(\text{H}_2) \approx 0.046 \text{ cm}^{-3} / 3 \times 10^{-4} \approx 150 \text{ cm}^{-3}$ and the analogous ratio for neutral particle excitation is of order unity. According to this line of argument OH should be a good thermometer, indicating $5 \text{ K} \lesssim T_{\text{K}} \lesssim 16 \text{ K}$ in the neutral-bearing region toward the star. This represents a paradox because a gas with its carbon fully ionized is unlikely to be this cold and densities $n(\text{H}_2) \approx 150 \text{ cm}^{-3}$ are far too small to excite CO at such very low temperatures. CO

requires an $n(\text{H}_2) \cdot T_{\text{K}}$ product which must at least be of order $n(\text{H}_2) T_{\text{K}} = 0.5 - 1.0 \times 10^4 \text{ cm}^{-3} \text{ K}$ (see Sect. 5).

There are now many cases where an expected high degree of electron excitation is simply not manifested in OH: its interstellar excitation temperature is measured to be within 0.5-1.0 K of the cosmic background in diffuse and translucent regions where electron and even neutral particle excitation should be substantial (Dickey, Kazès, and Crovisier 1981; Liszt and Lucas 1996). The anomalously low OH excitation temperatures seem to occur in the regime of the $\text{C}^+ \rightarrow \text{CO}$ transition (*ibid*). The factor $(T_{\text{ex}} - T_{\text{cmb}}) / T_{\text{ex}}$ in equation (1) can be very small for such weak excitation and, although it is possible that the OH abundance is really very low at the CO and HCO^+ peak to the South, this does not necessarily follow from the OH emission spectra. For column densities comparable to those seen around ζ Oph, $N(\text{OH})$ and $N(\text{HCO}^+)$ measured in absorption at radiofrequencies are very tightly related, with $N(\text{OH})/N(\text{HCO}^+) \approx 30$ (Lucas and Liszt 1996; Liszt and Lucas 1996); it is only OH emission that is weak, not $N(\text{OH})$ that is low.

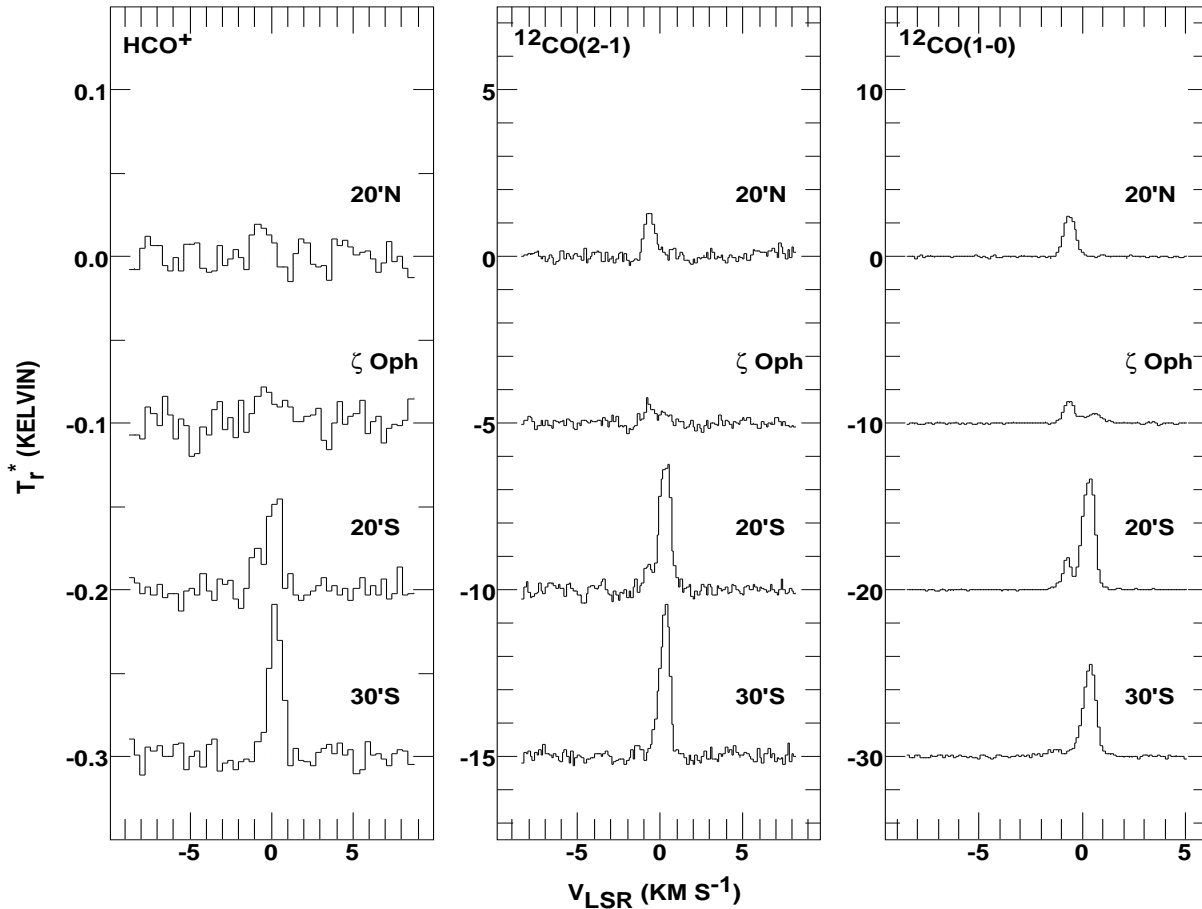


Fig. 5. Line profiles of HCO^+ , ^{12}CO $J=1-0$, and $J=2-1$ around ζ Oph. The resolution and channel spacing are 0.33 km s^{-1} for HCO^+ and 0.13 km s^{-1} for either CO line.

The model of Kopp et al. (1996) predicts an undetectably low abundance $N(\text{OH}) \lesssim 4 \times 10^{11} \text{ cm}^{-2}$ in the southerly gas, seemingly in accord with our data. Yet this situation is intimately related to their model's prediction $N(\text{HCO}^+) \approx 10^9 \text{ cm}^{-2}$, which they note is nearly a factor 1000 too low (see Liszt and Lucas 1994 and Sect. 4.1 here); HCO^+ should be made via the reaction of $\text{C}^+ + \text{OH}$ (Black and van Dishoeck 1986). It remains to be seen why the abundance of OH would be 100 times larger to the North, where its emission is easily seen, while the CO and HCO^+ are only slightly weaker there. But a problem remains either with the chemistry of OH or with its excitation.

3.3. Comparison of OH, CH and CO emission

3.3.1. CH and CO

Fig. 4 shows line profile integrals for these species taken separately over positive and negative velocities; upward pointing symbols are used to denote those positions at or to the North of ζ Oph. In the left-most panel, the CO line brightness is seen to increase greatly over narrow ranges of the CH profile integral. If the CH emission is a good surrogate for the column density $N(\text{H})$ (which CO most certainly is not), this behaviour

can probably be understood as the rapid onset of self-shielding (van Dishoeck and Black 1986, 1988; Kopp et al. 1996) which accompanies the $\text{C}^+ \rightarrow \text{CO}$ transition. It seems to occur in two branches for the Northern and Southern gas, perhaps related to differing positions with respect to the star (or the ambient uv flux in general), and there is an element of anti-correlation as well; the branch with stronger CH emission is somewhat weaker in CO. A particularly vivid example of the rapid rise expected of the CO intensity with changing $N(\text{H})$ or A_V is given by Kopp et al. (1996), whose Fig. 9 greatly resembles Fig. 4 here.

Similar behaviour is apparent in comparisons of CO with HCO^+ seen in absorption toward extragalactic continuum sources (Lucas and Liszt 1996), at $N(\text{HCO}^+) \approx 1-2 \times 10^{12} \text{ cm}^{-2}$. Here the analogous behaviour occurs at $\int T_A(\text{CH}) dv = 0.03-0.06 \text{ K km s}^{-1}$. If we scale from the observations toward ζ Oph, in which $\int T_A(\text{CH}) dv = 0.092 \text{ K km s}^{-1}$ corresponds to $N(\text{CH}) = 2.3 \times 10^{13} \text{ cm}^{-2}$, the CO turn-on occurs at $N(\text{CH}) = 0.75-1.5 \times 10^{13} \text{ cm}^{-2}$, with $N(\text{CH})/N(\text{HCO}^+) \approx 8$. Federman et al. (1994) show that higher values of $N(\text{CO})$ may occur at $N(\text{CH}) \gtrsim 3 \times 10^{13} \text{ cm}^{-2}$ in absorption spectra.

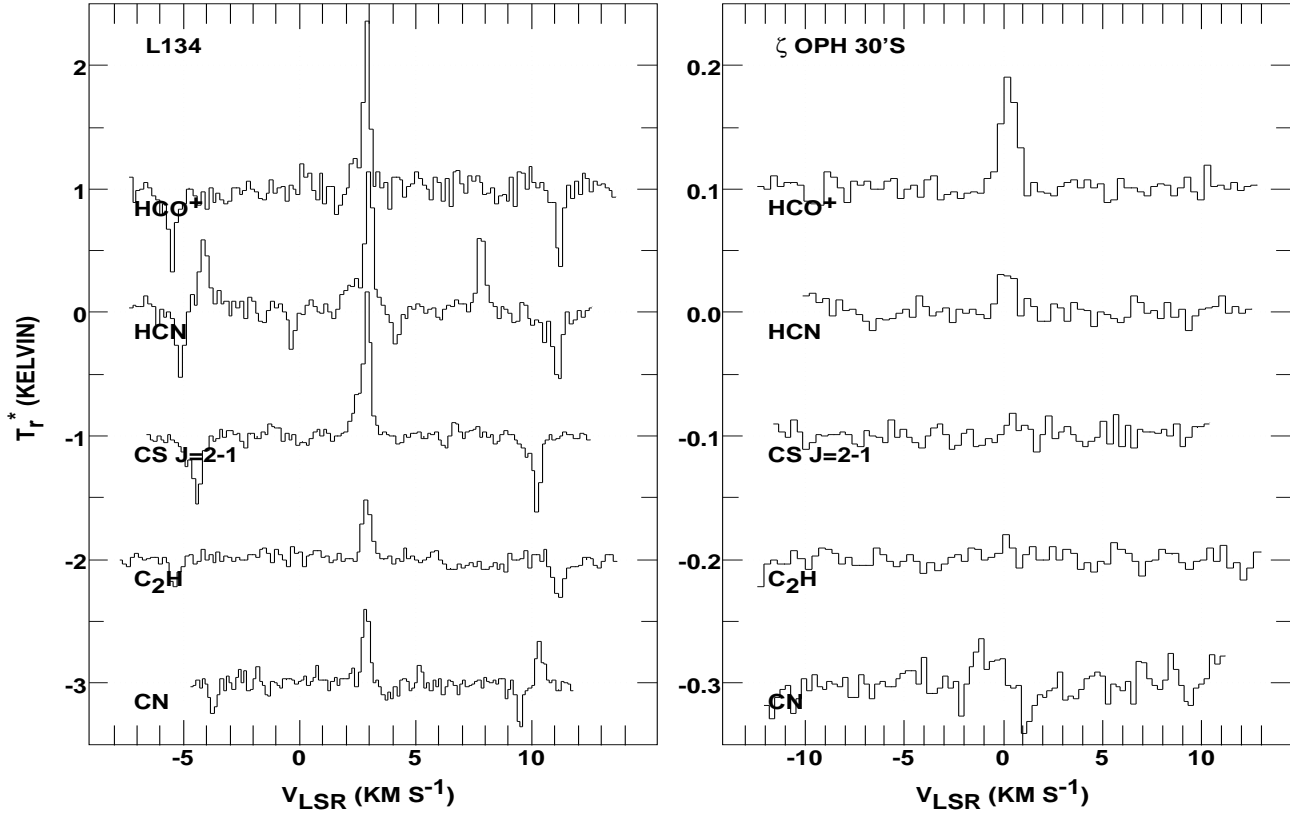


Fig. 6. Right: Line profiles observed at the CO and HCO^+ emission peak 30' S of ζ Oph in 100 kHz channels. Left; Observations of the same species toward L134 are shown for comparison but at 48 kHz resolution. The lines toward ζ Oph are substantially broader.

Table 1. Line profile integrals (K km s^{-1}) around ζ Oph

Position	CH	OH	$^{12}\text{CO}(1-0)$
80'S			5.00(0.05)
70'S			4.51(0.06)
60'S			2.05(0.04)
50'S			2.89(0.04)
40'S	0.091(0.011)	0.054(0.009)	4.61(0.04)
30'S	0.063(0.014)	0.051(0.012)	4.74(0.05)
20'S	0.085(0.011)	0.076(0.010)	6.03(0.02)
10'S	0.068(0.008)	0.092(0.006)	3.06(0.03)
ζ Oph	0.092(0.010)	0.103(0.006)	1.47(0.02)
10'N	0.104(0.012)	0.095(0.008)	2.14(0.03)
20'N	0.093(0.013)	0.134(0.011)	1.85(0.02)
30'N	0.084(0.014)	0.106(0.010)	3.00(0.02)
40'N	0.072(0.017)	0.099(0.009)	1.40(0.02)
50'N			1.60(0.02)
60'N			1.20(0.02)
70'N			0.72(0.03)
80'N			0.30(0.03)

3.3.2. CO and OH

This is shown in the middle panel of the Fig. 4 triptych. Those points corresponding to the weaker branches of the CO emission (*i.e.* $v < 0 \text{ km s}^{-1}$ to the South and $v > 0 \text{ km s}^{-1}$ to the

North) are shown greyed. For them, and for most of the data, the range of OH profile integrals is scarcely greater than the expected noise envelope while the CO integral varies by nearly a factor of 20. The remainder of the points, those corresponding to the dominant branch of the CO emission, appear to exhibit the inverse relationship which hides the strongest CO lines in OH. As discussed next, distinguishing between the weaker and stronger CO branches is necessary to understanding the relationships between CH and OH, which may be correlated or anticorrelated.

3.3.3. CH and OH

Overall, there may seem to be little apparent relationship between the line profile integrals of these species: with the possible exception of 1 outlying point, the CH-OH comparison at the right in Fig. 4 at first shows only scatter. This is due to the superposition of data showing two opposite kinds of behaviour. The points corresponding to the weaker CO component at each position, shown as the greyed, upward-filled and downward-open triangles at intermediate $\int T_A(\text{OH})dv$ and smaller $\int T_A(\text{CH})dv$, show a decline in OH as CH strengthens. Those points belonging to the dominant CO emission branches (*i.e.* $v > 0 \text{ km s}^{-1}$ to the South and $v < 0 \text{ km s}^{-1}$ to the North) show a rapid increase in the OH brightness with increasing $\int T_A(\text{CH})dv$, but in such a way as to preserve the inverse relationship between OH and

Table 2. $\int T_r^* dv$ (K km s⁻¹) for HCO⁺ and CO

Position	HCO ⁺	CO(1-0)	CO(2-1)	¹³ CO(1-0)
30' S	0.089(0.006)	4.74(0.05)	3.59(0.09)	
20' S	0.071(0.006)	6.03(0.02)	3.68(0.09)	0.137(0.013) ^a
10' S		3.06(0.03)	1.09(0.08)	0.061(0.013)
ζ Oph	0.034(0.009)	1.47(0.02)	0.70(0.06)	
20' N	0.025(0.006)	1.85(0.02)	1.13(0.07)	0.068(0.014)
30' N		3.00(0.02)	1.58(0.07)	0.106(0.017)

$$^a \int T_r^*(\text{C}^{18}\text{O})dv = 0.013 \pm 0.004 \text{ (K km s}^{-1}\text{)}$$

CO. For that subset of points showing this rapid growth of OH, the strongest CO lines are those with weaker CH (see 3.3.1).

In 3.2 we noted that $N(\text{OH})/N(\text{HCO}^+) \approx 30$ as seen in absorption in the radio regime while $N(\text{CH})/N(\text{HCO}^+) \approx 8$ is inferred from the existence of a rapid increase in $N(\text{CO})$ with either $N(\text{CH})$ or $N(\text{HCO}^+)$. The ratio which results from the comparisons with HCO⁺, $N(\text{OH})/N(\text{CH}) \approx 4$, is about what is seen toward ζ Oph optically, *i.e.* $N(\text{OH})/N(\text{CH}) \approx 2$.

4. Chemical abundances in the gas around ζ Oph

The first suggestions that a complex chemistry might be visible in the gas around ζ Oph were the CS observations of Drdla et al. (1989) and the detection of HCO⁺ emission by Liszt and Lucas (1994); this latter work was apparently the first time that polyatomic molecules were detected in a classical diffuse cloud. The column density of HCO⁺, $N(\text{HCO}^+) \approx 10^{12}$ cm⁻², is found to be 20 (van Dishoeck and Black 1986) to 1000 (Federman et al. 1996, Kopp et al. 1996) times higher than predicted by conventional quiescent chemical models, even when the abundances of CO, OH, and/or CH are reproduced.

To pursue the matter further we mapped the HCO⁺ emission somewhat better and searched for other species at the peak of the CO and HCO⁺ emission distribution to the South of the star. The point is that neither $N(\text{H})$ nor A_V is necessarily very much higher to the South than toward the star and even $N(\text{CO})$ and $N(\text{HCO}^+)$ may be constant within a factor two or so, with the emission pattern determined largely by excitation conditions. If so, the chemical patterns seen to the South may be interesting not only in their own right, but as guidelines to more complex phenomenon toward ζ Oph as well.

As shown in Fig. 5 and Table 1 the HCO⁺ emission roughly follows that of CO, but it is relatively strong toward the star and weak to the North. The CO J=2-1/J=1-0 intensity ratio is noticeably larger at the position 30' South, which is a clear indication that the excitation is stronger there. The weaker HCO⁺ lines are really at the limit of what one can expect to map with current technology.

4.1. Emission and column densities at the HCO⁺ emission peak

Emission profiles at the HCO⁺ peak are shown in Fig. 5 and summarized in Table 3. Toward L134, and at many scattered positions along the inner regions of the northern galactic plane at $l \lesssim 40^\circ$ (Liszt 1995), HCO⁺, HCN, CS (J=2-1), and C₂H

Table 3. $\int T_r^* dv$ (K km s⁻¹) 30' South of ζ Oph

Species	rms	$\int T_r^* dv$	f ^a
HCO ⁺	0.0067	0.089(0.006)	1.00
HCN	0.0055	0.032(0.005)	0.55
C ₂ H	0.0063	0.014(0.006)	0.42
CS	0.0060	0.007(0.006)	1.00
CN	0.0118	-0.001(0.009)	0.33

^a fraction in the strongest hyperfine component in LTE

Table 4. Logarithmic column densities 30' S of ζ Oph

T _K	n(H ₂)	X(e)=3 × 10 ⁻⁴				
		CO	HCO ⁺	HCN	CS ^a	CN ^a
10	3400	16.00	11.24	11.43	11.38	12.15
20	1350	15.65	11.54	11.66	11.65	12.35
30	800	15.65	11.76	11.84	11.76	12.50
40	620	15.65	11.87	11.95	11.80	12.56
60	360	15.65	12.10	12.16	11.96	12.72
X(e)=1 × 10 ⁻⁴						
10	3400	16.00	11.55	11.81	11.75	12.44
20	1350	15.65	11.83	12.05	11.81	12.62
30	800	15.65	12.04	12.24	12.01	12.74
40	620	15.65	12.15	12.33	12.03	12.78
60	360	15.65	12.39	12.55	12.11	12.90
X(e)=1 × 10 ⁻⁵						
10	3400	16.00	11.93	12.48	12.30	12.78
20	1350	15.65	12.14	12.66	12.24	12.87
30	800	15.65	12.29	12.79	12.23	12.93
40	620	15.65	12.36	12.85	12.18	12.96
60	360	15.65	12.53	13.01	12.22	13.02

^a 2 σ upper limit

emission profiles have similar brightnesses (accounting for hyperfine structure in species like C₂H); the same is true for CN in L134 as well. Typically such species are about 10 times weaker than ¹³CO (J=1-0) and 50 times weaker than ¹²CO. For HCO⁺ the lines seen around ζ Oph seem to follow this latter rule of thumb; they are 1%-2% as strong as ¹²CO (see Table 2).

This common similarity of the emission brightness in so many species seems a remarkable coincidence but it is certainly not repeated 30' South of ζ Oph. There, HCO⁺ is at least an order of magnitude stronger than CS and more than three times stronger than the main HCN line. The bump in the CN spectra is noise, unless it is supposed that the velocity of CN is unique; this is demonstrably not so toward the star (in optical spectra at least).

To interpret these line profiles in terms of molecular column densities we follow the $n(\text{H}_2) - T_K$ solution locus determined from ¹²CO and ¹³CO profiles of the J=2-1 and J=1-0 lines by Liszt (1993), shown in Table 4. As noted by Liszt (1993) the CO column density is well-determined as long as the gas is not at the high-density, low-temperature limit; the data of Kopp et al. (1996) yield very similar values of $N(\text{CO})$. In any case, even the maximum possible CO column density is small compared

to $N(\text{C}^+)$ toward the star ($2 \times 10^{17} \text{ cm}^{-2}$; Cardelli et al. 1993). It is not even necessarily large compared to the CO column seen there, $\log N(\text{CO}) = 15.4$.

The optically determined electron fraction, measured relative to H_2 is $X(e) = n(e)/n(\text{H}_2) \gtrsim 2\xi_{\text{C}} \gtrsim 2.6 \times 10^{-4}$ (Cardelli et al. 1993). Because the maximum allowed CO column density is still quite small compared to the total amount of carbon toward the star, it seems unavoidable that the majority of the carbon is ionized and the electron fraction is near the relative abundance of carbon itself. Thus only the largest of the parameterized choices of $X(e)$ is really relevant and the uncertainty in derived column densities is not as great as the full range of entries in the tables might otherwise suggest. The calculations with negligible $X(e)$ are included to illustrate the effect of neglecting the electron excitation when it is important.

For the species having higher dipole moments, we have performed excitation calculations using the electron-ion and electron-neutral rate constants of Bhattacharayya, Bhattacharayya, and Narayan (1981) and Dickinson and Flower (1981). We used the H_2 -molecule excitation rates of Green and Chapman (1978) and Turner et al. (1992) for CS and those of Monteiro (1985) for HCO^+ . For CN, following the recommendations of Turner et al. (1992), we used the same rate constants as for CO, from Flower and Launay (1985). For CN and HCN, where the lines are split, the calculations were done for the strongest component only since line overlap does not occur and the neutral cross-sections are not always known in detail anyway, especially for the admixture of atomic hydrogen which may be present.

The CO solution locus asymptotically but quickly reaches conditions of constant thermal pressure and column density when $T_{\text{K}} > T_{\text{ex}}$. It is this phenomenon, easily applied when the CO column density and excitation temperature are known, which first suggested that the density in the neutral-bearing clouds was small toward the star (Smith, Krishna Swamy and Stecher 1978; Liszt 1979). Species having higher dipole moments do not follow this behaviour if electrons provide significant excitation, as expected here. Unlike the CO solutions, those for the other species require higher molecular abundances at higher T_{K} , for two reasons; the density indicated by the CO solution locus declines at higher temperature and fixed pressure, lowering the density of electrons, and the electron excitation is itself less effective owing to an inverse-square root functional dependence on the kinetic temperature.

At the highest and most relevant electron fraction, the abundances or upper limits for HCO^+ , HCN, CS, and CN vary by a factor of five or so. The CO column density changes little for $T_{\text{K}} > 15\text{K}$ and the lowest-temperature (10 K) highest-pressure solutions probably can be excluded by a comparison of the ^{12}CO and ^{13}CO linewidths (Sect. 5; the ^{12}CO is not saturated). It is clear that HCN is at most only slightly more abundant than HCO^+ , and that CS is not as abundant as HCO^+ or HCN. Furthermore, the column density of CN is at most only slightly larger than toward the star ($\log N(\text{CN}) = 12.45$; van Dishoeck and Black 1989), although it might be the most abundant of the mm-wave species observed here. The range of HCO^+ col-

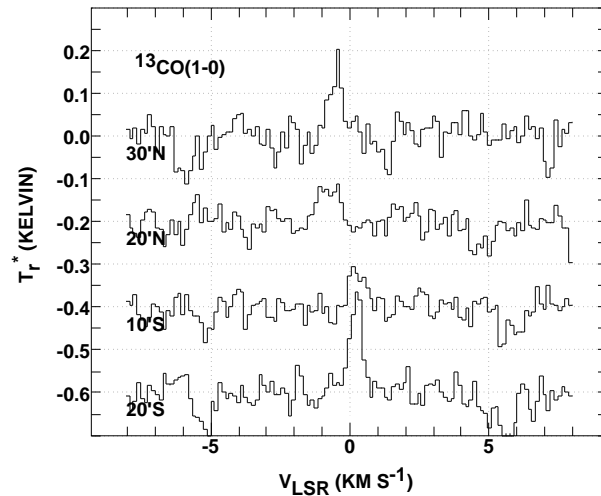


Fig. 7. Line profiles of ^{13}CO $J=1-0$ emission observed at 4 positions directly North and South of ζ Oph. The channel spacing and resolution are 0.13 km s^{-1} .

umn densities in Table 3 is wider but fully overlapped with that inferred by Liszt and Lucas (1994) toward the star.

Drdla et al. (1989) presented a detection of CS $J=2-1$ emission toward ζ Oph with $\int T_{\text{A}} dv = 0.02 \pm 0.005 \text{ km s}^{-1}$ and a peak intensity $T_{\text{A}} = 0.013 \pm 0.003 \text{ K}$; their quoted CS column density $N(\text{CS}) = 0.7 - 5.0 \times 10^{12} \text{ cm}^{-2}$ is substantially larger than the limits we set at the molecular emission peak to the South (Table 3). Their line profile occupies the range $-3 \text{ km s}^{-1} < v < -1 \text{ km s}^{-1}$, which does not overlap with emission from any other species. Our CS $J=2-1$ spectrum toward ζ Oph is featureless. Over the velocity range corresponding to the CO $J=1-0$ emission profile, our data have rms noise $\Delta \int T_{\text{r}}^* dv = 0.006 \text{ K}$.

5. CO isotope ratio, excitation, and H_2 conversion factor

Comparison between the carbon isotope ratios observed in CO and in the gas phase generally should be a powerful diagnostic: the fractionation reaction of ^{12}CO and $^{13}\text{C}^+$ (Watson, Anicich, and Huntress 1976), with an exothermicity corresponding to 35 K, should act powerfully to enhance the abundance of ^{13}CO at low temperatures (Crutcher and Watson 1981). Knowledge of the $^{12}\text{CO}/^{13}\text{CO}$ isotope ratio could serve to discriminate between low and high temperature solutions at the HCO^+ emission peak, because only the low-temperature, high-density, very optically thick solutions for CO are compatible with $^{12}\text{CO}/^{13}\text{CO}$ ratios substantially larger than those given by the profile integrals directly (*i.e.* 30-50). Ordinarily one might rely on *Copernicus* or *HST* CO absorption line data to settle this matter but questions of the proper wavelength assignments of some rotation-vibration bands (Haridass and Huber 1994) have resulted in values ranging from $N(^{12}\text{CO})/N(^{13}\text{CO}) = 55 \pm 11$ (Wannier et al. 1982) and 82 ± 25 (Lyu et al. 1994) to 167 (Lambert et al. 1994).

Toward the star in the $J=1-0$ line, Wilson et al. (1992) find $T_{\text{r}}^*(^{12}\text{CO})/T_{\text{r}}^*(^{13}\text{CO}) \gtrsim 110$, superseding the older value of 70 ± 30 from Langer, Glassgold and Wilson (1987). We reported

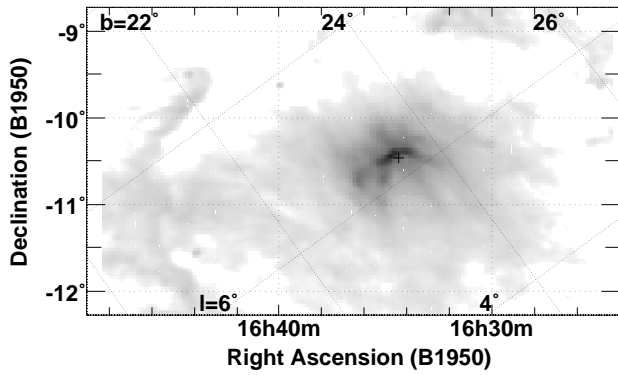


Fig. 8. 60μ IRAS image of the region around ζ Oph showing its bow shock. The position of the star is marked by a cross. 1° corresponds to 2.44 pc at a distance of 140 pc.

(Liszt 1992, 1993) that this ratio is surprisingly high ($\gtrsim 30$) at the emission peaks $20'$ - $30'$ to the North and South: the more sensitive new ^{13}CO data shown in Fig. 7 and summarized in Table 2 confirm this (see also Kopp et al. 1996). To the South, in the higher velocity line, the intensity ratios are 44 ± 4 and 50 ± 12 . To the North, they are 28 ± 6 and 29 ± 5 . Clearly the isotopic intensity ratio varies widely over the central $20'$, with a very strong peak toward the star. Unless the optical depth is much lower there, the isotopic abundance ratio must also change by roughly similar amounts.

^{12}CO J=1-0 emission toward ζ Oph cannot be too optically thin unless it is very different from that seen in absorption. Adopting the column density and rotational populations recently measured in uv -absorption leads to values for the integrated optical depth of the J=1-0 line which are 0.9 – 1.4 km s^{-1} . If the optical depth is distributed over an intrinsic profile which resembles the CO emission (which itself is very similar to the absorption-line profiles of species besides CH^+), the peak optical depth is 1.2 – 2.0 . The higher optical depth corresponds to an excitation temperature of 4.5 K and a 1.2 K emission line brightness, the lower to an excitation temperature slightly over 6 K and a CO J=1-0 emission line which is perhaps somewhat brighter ($T_{\text{B}} = 2.1 \text{ K}$) than observed. For the excitation solution with $\tau = 2$, the isotopic abundance ratio should be (only) 40% larger than the intensity ratio.

At the position $20'$ South, the linewidths (FWHM) of the stronger J=1-0 components are $0.65 \pm 0.01 \text{ km s}^{-1}$ and $0.50 \pm 0.04 \text{ km s}^{-1}$ for ^{12}CO and ^{13}CO respectively. If the weaker line is optically thin, this difference in linewidth can be explained entirely if the line center optical depth in ^{12}CO is in the range 2.0 – 2.5 . This scant difference in width precludes heavy saturation of the ^{12}CO profile and eliminates those excitation solutions in which the temperature is low and the carbon isotope ratio is as large as, say, 167 (Lambert et al. 1994)². We conclude that the emission measurements are consistent with the very large $^{12}\text{CO}/^{13}\text{CO}$ ratio found in optical absorption toward the star, but

² There is also no evidence in the emission profiles for a segregation of the ^{13}CO to a more limited and hence kinematically-narrower region

that such a large ratio is not characteristic of the immediately adjacent gas sampled in emission $10'$ away; the ^{12}CO optical depth is too small.

The ^{13}CO lines are strong enough in some positions so that might hope to detect C^{18}O . If the $^{13}\text{CO}/\text{C}^{18}\text{O}$ intensity ratio were found to be unusually small, this might support a supra-terrestrial $^{12}\text{C}/^{13}\text{C}$ isotope ratio. A search for C^{18}O by Kopp et al. (1996) yielded $N(^{13}\text{CO})/N(\text{C}^{18}\text{O}) > 5$ at one position. Our data (Table 2) $20'$ South of the star yield a value ≥ 10.5 for the ratio of line strengths at the $3\text{-}\sigma$ level. Given the low optical depths in both lines, this intensity ratio cannot differ greatly from that of the abundances themselves.

5.1. CO excitation and the CO- H_2 conversion factor in diffuse gas

The weak rotational excitation and low thermal pressure $n(\text{H}_2)T_{\text{K}} = 0.5 - 1.0 \times 10^4 \text{ cm}^{-3} \text{ K}$ inferred from the small CO J=1-0 excitation temperature toward the star (Smith, Krishna Swamy, and Stecher 1978; Liszt 1979) are confirmed by mm-wave emission observations of the unseen CN (Crane et al. 1989) and CO J=3-2 lines (van Dishoeck and Black 1991) but not by a comparison of the ^{12}CO J=2-1 and J=1-0 emission lines (Crutcher and Federman 1987). Although there is a fair range of ratios in the literature, the thermal pressure inferred from a comparison of the two lowest CO lines is typically $p/k = 1 - 2 \times 10^4 \text{ cm}^{-3} \text{ K}$. Similar or slightly higher pressures may be derived from the uv absorption-line column densities of Lambert et al. (1994) who found excitation temperatures of 3.9 ± 0.4 , 4.6 ± 0.2 and $6.3 \pm 0.5 \text{ K}$ for the lowest three rotation transitions. These excitation temperatures would produce an easily-detectable ($\approx 1\text{ K}$) J=3-2 line, in substantial disagreement with the results of van Dishoeck and Black (1991). Much weaker excitation and lower gas pressure are implied by the analysis of other uv absorption-line data of Lyu et al. (1994).

It seems undeniable that the CO profiles have wide swings in integrated intensity under conditions where neither A_{V} nor $N(\text{CO})$ changes much. Toward the star, $N(\text{H}_2)/\int T_{\text{r}}^*(\text{CO})dv = 6 \times 10^{20} \text{ cm}^{-2}/1.5 \text{ K km s}^{-1} = 8 \times 10^{20} \text{ cm}^{-2} (\text{K km s}^{-1})^{-1}$, which is 2-3 times larger than typically-employed values. However, at the emission peak to the South, the CO is four times stronger and the CO intensity- H_2 column density ratio is unexceptional or even somewhat low. This suggests that the common value is established fairly soon after CO emission turns on (Liszt 1982), even while $N(\text{CO})/N(\text{C}^+) \ll 1$.

6. Summary

Mapping of the large-scale emission patterns around ζ Oph shows that the CO emission components to the North and South of the star separately ‘turn on’ over narrow ranges of the CH line profile integral. We ascribe the rapid brightening of the CO line to the effects of a partial $\text{C}^+ \rightarrow \text{CO}$ conversion (Liszt 1992, 1993; Kopp et al. 1996) in a nearly-fixed total gas column, which in turn lends confidence to the assumption that CH traces the column density (Mattila 1986; Magnani and Onello 1995).

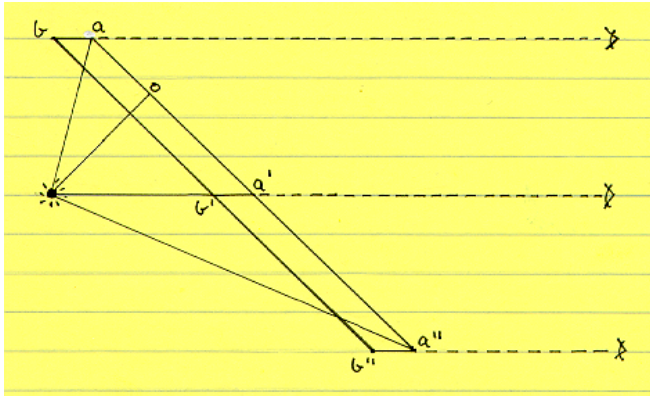


Fig. 9. A viewing geometry which creates a one-sided maximum in CO as the result of increased extinction.

For OH no such conclusion is reached, as our profiles fail to show not only the pre-shock gas at $+4.5 \text{ km s}^{-1}$ discussed by Crutcher (1979), but most of the stronger CO component as well. We attribute this to a more widely-identified problem with OH excitation in the regime of the $\text{C}^+ \rightarrow \text{CO}$ conversion (Dickey, Kazès, and Crovisier 1981; Liszt and Lucas 1996), whereby the excitation temperature is unaccountably small (see also Roueff 1996). However the excitation of CH is probably no better understood; its (typical) negative excitation temperature deduced toward the star should probably have been squelched by electron impact excitation. OH and CH emission vary proportionally and inversely for the stronger and weaker CO components, respectively.

Four spectra of HCO^+ emission show that it resembles CO and CH in its behaviour, peaking in both components, one on either side of the star. Given the close relationship between HCO^+ and OH in models of the chemistry, and as observed directly (Lucas and Liszt 1996; Liszt and Lucas 1996) there is no obvious explanation as to why the OH behaviour is so different in the northern and southern regions. Clearly there is a serious problem in understanding either the chemistry or the excitation of this molecule.

A search for CS, CN, HCN, and C_2H emission to the South of the star, where HCO^+ is strong, detected only HCN. We infer that the molecular abundances are not necessarily much larger than would be found toward the star, unless the gas is much colder to the South. We could not confirm the earlier detection of CS emission toward the star by Drdla et al. (1989). Limits on $N(\text{CS})$ at the Southern emission peak are typically an order of magnitude below those set optically by Snow (1976).

At four positions $10'$ - $30'$ from the star, we found that the isotopic intensity ratio $T_r^*(^{12}\text{CO})/T_r^*(^{13}\text{CO})$ is 30-50; such values are quite large considering the 3-6 K ^{12}CO brightnesses, but still much smaller than the ratio ≈ 110 found toward the star by Wilson et al. (1992). Given that the ^{12}CO optical depth is in the range 1-2 both toward the star and $20'$ to the South, large variations in the CO isotopic abundance ratio are indicated. The relative abundance of ^{13}CO increases as the CO lines brighten generally at outlying positions.

One of the most interesting questions is the existence of a strong minimum in the CO emission and ^{13}CO relative abundance very near the position of the star; ratios as large as $N(^{12}\text{CO})/N(^{13}\text{CO}) = 167$ are seen nowhere else, even at similarly-low $N(^{12}\text{CO}) = 2.4 \times 10^{15} \text{ cm}^{-2}$ (Lucas and Liszt 1997). The star is also the approximate center of a pattern of interesting kinematic symmetry, but, owing to the existence of a large surrounding HII region, the absorbing gas parcels are often considered to be quite distant from it. Then, the observed symmetries and other seemingly-unique behaviour are entirely accidental, like weather. On the other hand, if the star and gas were close, the star's local space velocity of some 100 km s^{-1} would move it past the clouds at the rate of 1 pc ($25'$) every 10^4 years. A time-series of absorption profiles could yield valuable insights into the small-scale structure of the absorbing gas (Liszt 1992).

ζ Oph is known to have a substantial bow shock (van Buren and McCray 1988; Fig. 8), and it is tempting to attribute this to interaction with neutral gas. Such shocks are actually quite common (*ibid*), but, if the star and neutral gas are not too distant from each other, there are a variety of simple geometries which yield some aspects of the observations—in this case, a CO minimum near the position of the star and strong one-sided increase away from it—with a minimum of contrivance. We rely on the fact that CO, which is on the verge of becoming strongly self-shielding toward the star, is expected to be strongly affected by even slight shifts in the photoionization rate and extinction (Kopp et al. 1996).

In Fig. 9 we show a case where a bright star, contributing much of the local uv -photoionization, is viewed through a thin, undisturbed slab of gas. The extinction across the near (to us) face of the slab, measured to the star, follows a cosecant law and is much higher at a'' than at o or a . Coupled with the inverse-square dependence of the radiation field (a'' is much more distant from the star than either o or a) the photoionizing flux across the front face of the cloud varies greatly and a strong, one-sided maximum would presumably be produced in CO. Much stronger emission would be expected at a'' than at a , even though both are seen equidistant from the star.

Acknowledgements. The National Radio Astronomy Observatory is operated by Associated Universities, Inc. under a cooperative agreement with the National Science Foundation.

References

- Allen, M. 1994, ApJ, 424,754
- Bhattacharayya, S. S., Bhattacharayya, B., Narayan, M. V. 1981, ApJ, 297, 936
- Barlow, M. J., Crawford, I. A., Diego, F., Dryburgh, M., Fish, A. C., Howarth, I. D., Spyromilio, J., Walker, D. D. 1995, MNRAS, 272, 333
- Bertojo, M., Cheung, A., Townes, C. H. 1976, ApJ, 208, 914
- Bouloy, D., Omont, A. 1978, A&A, 61, 405
- Cardelli, J. A., Mathis, J. S., Ebbets, D. C., Savage, B. D. 1993, 402, L17
- Crane, P., Hegyi, D., Kutner, M. L., Mandolesi, N. 1989, ApJ, 346, 136
- Crawford, I. A. 1996, MNRAS, 280, 863.

- Crawford, I. A., Barlow, M. J., Dryburgh, M., Spyromilio, J. 1994, MNRAS, 266, 903
- Crawford, I. A. 1995, MNRAS, 277, 458
- Crutcher, R. M. 1979, ApJ, 231, L151
- Crutcher, R. M., Watson, W. D. 1981, ApJ, 244, 855
- Crutcher, R. M., Federman, S. R. 1987, ApJ, 316, L171
- de Geus, E. J., Bronfman, L., Thaddeus, P. 1990, A&A, 231, 137
- de Geus, E. J., Burton, W. B. 1991, A&A, 246, 559
- Dickey, J. E., Crovisier, J. and Kazès, I. A&A, 98, 271
- Dickinson, A. S., Flower, D. R. 1981, MNRAS, 196, 297
- Drdla, K., Knapp, G. R., van Dishoeck, E. F. 1989, ApJ, 345, 815
- Falgarone, E., Pineau des Forêts, G., Roueff, E. 1995, A&A, 300, 870
- Federman, S. R., Willson, R. F. 1982, ApJ, 260, 124
- Federman, S. R. et al. 1994, ApJ, 424, 772
- Federman, S. R. 1996, Rawlings, J. M. C., Taylor, S. D., Williams, D. A. 1996, MNRAS, 279, L41
- Flower, D. R., and Launay, J. M. 1985, MNRAS, 214, 271
- Green, S., Chapman, S. 1978, ApJS, 37, 169
- Haridass, C., Huber, K. P. 1994, ApJ, 420, 433
- Hobbs, L. M. 1969, ApJ, 157, 135
- Hobbs, L. M. 1973, ApJ, 180, L79
- Hogerheijde, M. R., de Geus, E. J., Spaans, M., van Langevelde, H. J., van Dishoeck, E. F. 1995, ApJ, 441, L93
- Koch, A., van Hemert, M. C., van Dishoeck, E. F. 1995, JCP, 103, 7006.
- Kopp, M., Gerin, M., Roueff, E., Le Boulrot, J. 1996, A&A, 305, 558
- Lambert, D. L., Sheffer, Y., Crane, P. 1990, ApJ359, L19
- Lambert, D. L., Sheffer, Y., Gilliland, R. L., Federman, S. R. 1994, ApJ, 420, 756
- Langer, W. D., Glassgold, A. E., Wilson, R. W. 1987, ApJ, 322, 450
- Lien, D. 1984, ApJ, 284, 578
- Liszt, H. S. 1979, ApJ, 233, L147
- Liszt, H. S. 1982, ApJ, 262, 198
- Liszt, H. S., 1992, ApJ, 390, 226
- Liszt, H. S., 1993, ApJ, 414, 242
- Liszt, H. S., 1995, ApJ, 442, 163
- Liszt, H. S., Lucas, R. 1994, ApJ, 431, L131
- Liszt, H. S., Lucas, R. 1995, A&A, 299, 847
- Liszt, H. S., Lucas, R. 1996, A&A, in press (available on-line at <http://www.cv.nrao.edu/~hlszt>)
- Lucas, R., Liszt, H. S. 1996, A&A, 307, 237
- Lucas, R., Liszt, H. S. 1997, in preparation
- Lyu, C.-H., Smith, A. M., Bruhweiler, F. C. 1994, ApJ, 426, 254
- Magnani, L., Onello, J. S. 1995, ApJ, 443, 169
- Mattila, K. 1986, A&A, 160, 157
- Morton, D. C. 1975, ApJ, 197, 85
- Monteiro, T. S. 1985, MNRAS, 214, 419
- Roueff, E. 1996, MNRAS, 279, L37
- Savage, B. P., Cardelli, J. A., Sofia, U. J. 1992, ApJ, 401, 706
- Sheffer, Y., Federman, S. R., Lambert, D. L., Cardelli, J. A. 1992, ApJ, 297, 482
- Smith, A. M., Krishna Swamy, K. S., Stecher, T. P. 1978, ApJ, 220, 138
- Snow, T. P. 1976, ApJ, 204, L127
- Turner, B. E., Chan, K.-W., Green, S., Lubowich, D. 1992, ApJ, 399, 114
- van Buren, D., McCray, R. 1988, ApJ, 329, L93
- van Dishoeck, E., Black, J. H. 1986, ApJS, 62, 109
- van Dishoeck, E., Black, J. H. 1988, ApJ, 334, 771
- van Dishoeck, E., Black, J. H. 1989, ApJ, 340, 273
- van Dishoeck, E., Black, J. H. 1991, ApJ, 369, L9
- Wannier, P. G., Penzias, A. A., Jenkins, E. P. 1982, ApJ, 254, 100
- Watson, W. D., Anicich, V., Huntress, W. T. 1976, ApJ, 205, L165
- Wilson, T. L., Mauersberger, R., Langer, W. D., Glassgold, A. E., Wilson, R. W. 1992, A&A, 262, 248